Geoheritage (2025) 17:179
https://doi.org/10.1007/s12371-025-01233-y

ORIGINAL ARTICLE

Painted Pebbles of Southern Tuscany (Italy): A Journey from Natural Beauty to Mineralogical and Geochemical Insights

A. Orlando[1] · M. G. Benvenuti[2] · E. Pecchioni[2] · M. Ricci[3] · A. P. Santo[2]

Received: 23 May 2025 / Accepted: 19 November 2025

Abstract
This study investigates the textural and mineralogical features of unusually coloured pebbles, here referred to as *giottoli*, collected from hills, riverbanks, and coastal areas in southern Tuscany (Central Italy). Inspired by the curiosity of a non-specialist collector, Roberto Mari, these pebbles were analysed using various analytical techniques to understand the processes underlying their distinctive, art-like patterns. The *giottoli* display periodic colour banding across a wide chromatic range, mainly in shades of red, yellow, and grey, with varying intensities. X-ray diffraction, elemental mapping, and backscattered electron imaging revealed pronounced mineralogical zonation and significant compositional heterogeneity. Mineralogically, the pebbles primarily comprise quartz, calcite, and phyllosilicates (predominantly kaolinite). Red and yellow zones are enriched in iron oxyhydroxides (FeOx), notably hematite (restricted to red areas) and goethite. In contrast, grey areas exhibit low FeOx concentrations and limited alteration, potentially preserving original mineralogical signatures. The *giottoli* are interpreted as fine-grained sedimentary clastic rocks undergoing pressure solution processes (stylolitisation) and later mineralisation via carbonate veins. These features may have promoted FeOx precipitation through interaction with iron-rich fluids, likely linked to discharges from the Colline Metallifere mining district (Tuscany). During FeOx precipitation, cations (e.g. Si, Al, Ca, Mn) were incorporated and their abundance (in particular that one of Mn) may be responsible for the outstanding colour variability that makes these natural objects so fascinating. Based on their texture and composition, the *giottoli* are classified as siliciclastic mudstone. This study illustrates how public curiosity can inspire meaningful scientific investigation, offering new insights into geologic processes.

Keywords Tuscany · Pebbles · *Giottoli* · Colour banding · Fe oxyhydroxides · Fluid-rock interaction

Introduction

The social perception of Geology, at least in the western world, is at best not fully clear as in many cases the public confuses the activity of the geologists with those of archaeologists, architects, engineers and so on. In the worst case this diffuse perception is strongly negative attributing to the geologists and Geology, in general, the responsibility for unsustainable exploitation of natural resources, an active role in the anthropogenic climate crisis due to fossil energy and a weak capacity for prediction and mitigation of natural hazards. In both cases, a critical aspect related to such public perception is represented by ineffective communication of geoscientists toward human societies (Lacchia et al., 2020). Looking at a rock outcrop or sample, a geologist may reconstruct, through descriptive and analytical approaches, the complex interplay of physical, chemical, and biological processes which in space and time, drove and still regulate the dynamics of the Earth system. The rock in the geologist's eyes, represents the dance of energy and matter that, from 4.5 billion years, renews on Earth with effects that unfortunately are ever more perceived as producing negative or catastrophic impacts on our lives.

The present study has been stimulated by the curiosity and fascination of a person, Roberto Mari, unfamiliar with

✉ A. P. Santo
alba.santo@unifi.it

[1] C.N.R. – Istituto di Geoscienze e Georisorse – Sede di Firenze, via G. La Pira, 4, Firenze 50121, Italy

[2] Dipartimento di Scienze della Terra, Università degli Studi di Firenze, via G. La Pira 4, Firenze 50121, Italy

[3] Dipartimento di Chimica "Ugo Schiff", Università degli Studi di Firenze, via della Lastruccia 3, Sesto Fiorentino Firenze 50019, Italy

Published online: 03 December 2025

geological concepts and theories, who collects humble pebbles peculiar for their colours from hills, riverbanks and shorelines of southern Tuscany (Central Italy) (Mari 2018). To Roberto's eyes these pebbles, through their colour patterns (Fig. 1), represent a form of natural art as attested to by the term *giottoli* that he associated with them referring to the Tuscan Middle Age painter *Giotto da Bondone*. Roberto was looking for a scientific explanation of such a "rock art" and the present study summarizes a geological description and interpretation of these peculiar pebbles starting from the regional setting of their occurrence down to the mineralogical and geochemical analyses of their unusual, coloured and variable aspect. Together with the scientific results this study aims to stress the possibility of a positive relation between the public and geoscientists for improving our awareness of living on a dynamic planet just starting from the tale of a coloured pebble.

This study links the macroscopic observation of these distinctive pebbles with their detailed microscopic and geochemical investigation, presenting new analytical results and showing how aesthetic fascination can stimulate rigorous research and promote public appreciation of geoheritage, as exemplified by a coloured pebble.

The Geological Setting of the Painted Pebbles

The area where the painted pebbles have been collected lies mainly within the catchment of the Cornia River, covering a surface of about 365 km^2 from the source in the *Colline Metallifere* to the outlet along the Tyrrhenian coast south of Piombino (Fig. 2). This area is part of the internal portion of the Northern Apennines (NA), a collisional orogen developed throughout a full Wilson Cycle of plate dynamics. The latter started in the latest Paleozoic with the fragmentation of the Pangea supercontinent and the development of Triassic rifted basins progressively invaded by the sea during the Jurassic with the opening of a narrow northwestern arm of the Tethys Ocean, the Ligurian-Piedmont Ocean. Since the late Cretaceous, the Europe-Africa plate convergence started to close this narrow ocean, bringing during the early Cenozoic, after a complete ocean subduction, to the continent collision, initiating the development of the NA orogen. This complex evolution is regionally recorded by a pile of thrust and folded sedimentary, low-grade metamorphic and magmatic successions, also stacked in the reliefs of the study area, which records these adjacent palaeogeographic and geodynamic domains (Vai and Martini 2001; Conti et al., 2020).

Fig. 1 Examples of pebbles showing different size, colours and patterns. The white scale bar corresponds to 4 cm

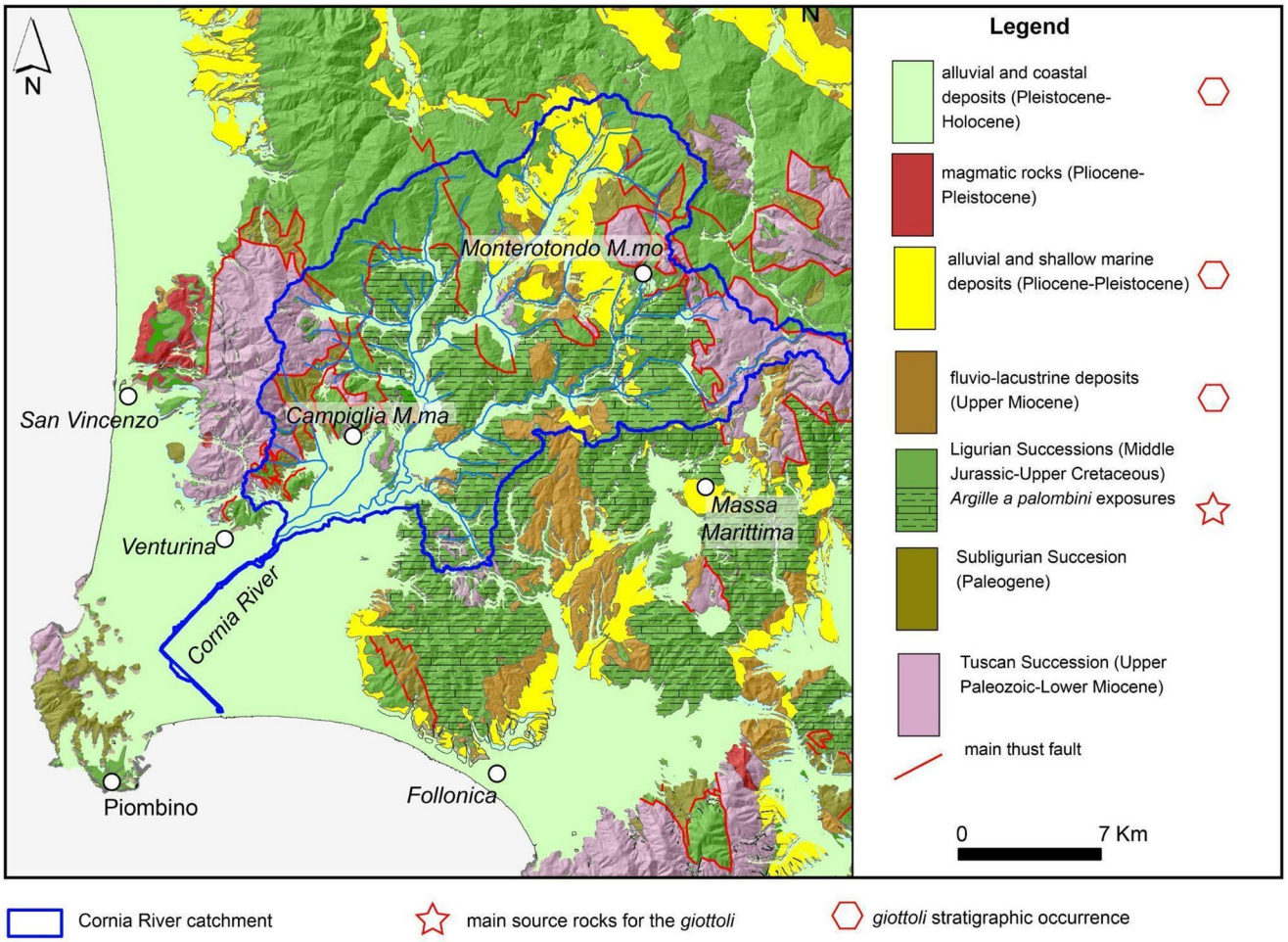

Fig. 2 Schematic structural map of the Cornia River catchment and surrounding areas. The Ligurian Successions include the *Argille a Palombini* Formation representing the main source for the *giottoli*

The succession representing the ocean realm includes slices of the ocean lithosphere (ophiolites) and thick terrigenous-cherty-carbonate pelagic and turbiditic deposits (Ligurian Succession; Conti et al., 2020). The ocean-continent transitional domain and the continental margin of the African plate are represented by terrigenous-carbonate deposits grouped respectively in the Subligurian and Tuscan successions (Conti et al., 2020). The Ligurian succession forms the top of the structural edifice of the NA chain thrust onto the Subligurian in turn tectonically in contact with the Tuscan successions. In the present southern Tuscany, the NA chain emerged since the late Tortonian, and underwent further stages of structural development marked by differential crustal movements alternatively attributed to extensional or compressional-extensional tectonic regimes (Martini and Sagri 1994; Bonini et al., 2014). Despite the contrasting structural interpretations, the late Neogene and the Quaternary were characterised by the activation and development of several intermontane basins filled fluvial-lacustrine and shallow marine mostly clastic successions (Martini and Sagri 1994). Concurrently with the differential uplift, magmatic phenomena affected a wide region between the current Tuscan archipelago and southern Tuscany (Peccerillo 2017). Magmas generated by crustal melting intruded at shallow depths the structural stack forming the relief of this region. In some cases, such as near present-day San Vincenzo on the coast and Roccastrada inland, magmas reached the surface, creating small volcanic centres that have been completely dismantled by erosion. The magmatic activity in southern Tuscany in the last million years entered a hydrothermal stage documented by diffuse polymetallic ore deposits and by the occurrence of geothermal reservoirs currently exploited as a source of renewable energy.

The studied pebbles have been collected by Roberto Mari from coarse-grained deposits stratigraphically distributed between the Messinian, in the inner portion of the catchment, and the Recent, in the present river thalweg and shorelines, attesting to a long-lived drainage network sourced from the relieves embracing the catchment of the Cornia River. These are made of the Ligurian succession

thrusted into the lowermost portion of the Tuscan succession. The lithological composition of the studied clasts is a dark grey-green, calcilutite containing varying amounts of silica deriving from strongly deformed strata ascribed to the Argille a Palombini Formation (uppermost Lower-Upper Cretaceous; Ghelardoni et al., 1965). This formation formed in basin plain deposits of the Ligurian-Piedmont ocean floor straddling the Calcium Compensation Depth.

Materials and Analytical Techniques

Materials

The *giottoli* consist of pebbles displaying different coloured areas, sometimes forming rhythmic bands or folds which are, in some cases, intersected by submillimetric to millimetric (<2 mm) veins. The colours of the pebbles are striking and varied, ranging from red to yellow and grey, and from green to blue and purple. The coloured areas give rise to geometric patterns or complex motifs that evoke waves, clouds, or efflorescences, resampling abstract forms of painting at a very small scale (Fig. 3a, b). The variation in colours and shapes occurs on such a small scale that a single pebble, just a few centimetres thick, presents a very different appearance depending on whether it is observed on one side or the other (Fig. 3a, c). The transition from one colour to another is sometimes gradual and sometimes abrupt (Figs. 3, 4 and 5).

The data reported in this paper were derived from *giottoli* samples exhibiting three colours, grey, red, and yellow, with varying degrees of intensity. Examples of the studied samples are shown in Fig. 4.

Analytical Techniques

The study of the pebbles was conducted on ten samples using various analytical techniques that enabled their examination at different scales. Initially, all ten samples were considered; they were observed under the optical microscopy and analysed by XRDP. Additional analyses (calcimetry, pXRF, EPM, Raman, see below) were carried out on a smaller subset (1–3 samples).

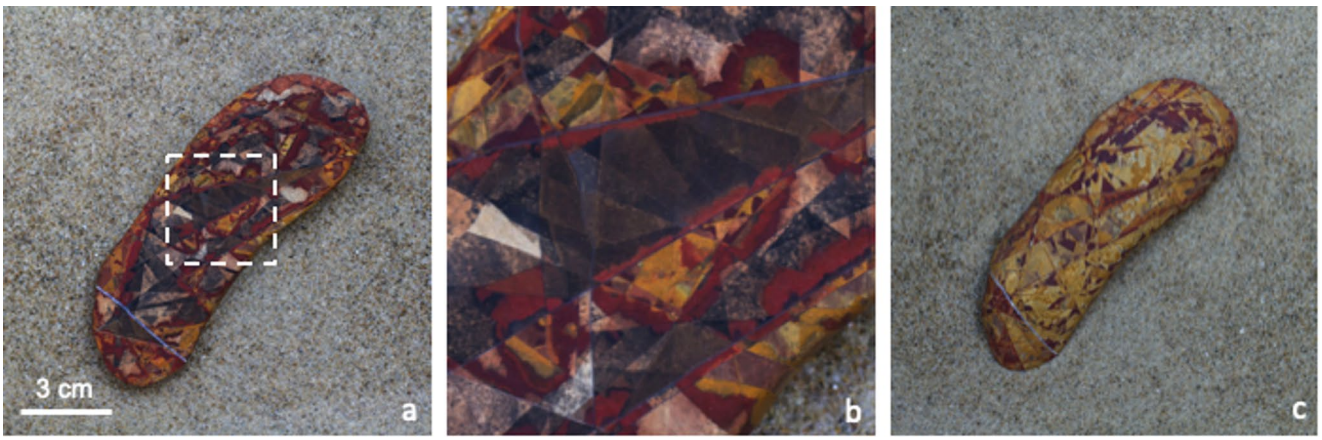

Fig. 3 Picture of a pebble **(a)**, a detail (boxed area in the Fig. 3a) showing a complex pattern of shapes and colours **(b)**, and the same pebble as seen from the other side **(c)**

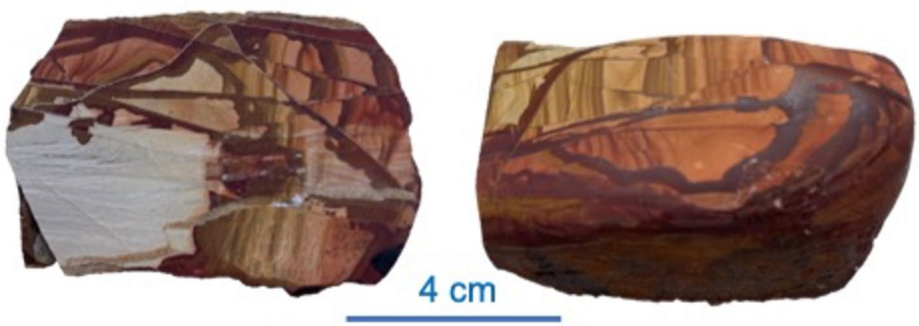

Fig. 4 Examples of the studied pebbles

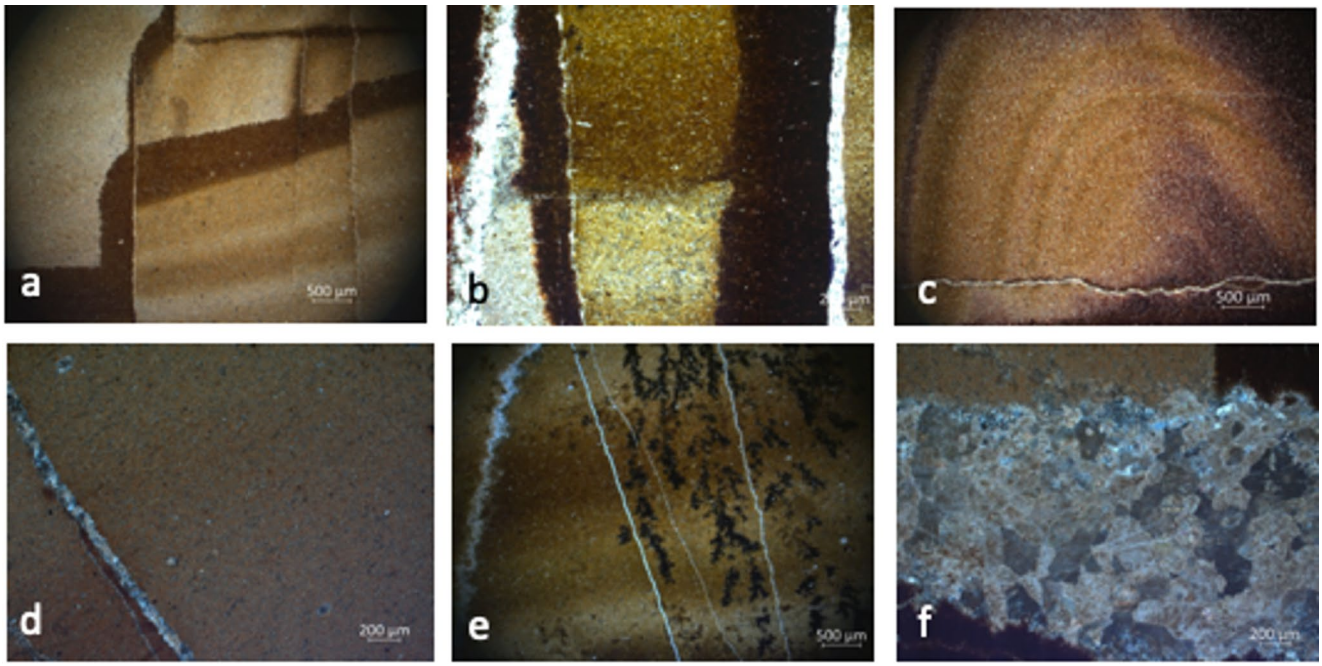

Fig. 5 Microphotographs taken using a polarizing microscope with parallel nicols. The images show colour bands (a, b, c), veins of varying size (a-f), small quartz crystals (d), and dendrites (e)

Optical Microscopy (PLM)

Petrographic observations in polarised light (PLM) were performed using a Zeiss Axioscope A.1 microscope (Carl Zeiss, Jena, Germany), equipped with a 5 Megapixel resolution video camera and Zen lite 3.1 image analysis software. This analysis allows for the characterisation of the texture and the mineralogical composition of the samples.

X-Ray Powder Diffraction (XRDP)

Mineralogical qualitative analyses were performed on ten samples using X-ray powder diffraction (XRPD) on powder samples, using a Philips PW 1050/37 diffractometer (Philips, Almelo, The Netherlands), coupled with a Panalytical X'Pert PRO and HighScore software data acquisition and interpretation system. The detection limit for this method is 4%. The operating conditions were 40 kV-20 mA, Cu anode, graphite monochromator, and a 2°/min goniometer speed, with a scanning range between 5°–70° 2Θ.

Calcimetry

$CaCO_3$ was determined by the Dietrich-Fruhling Calcimeter which consists of a sealed glass container where the reaction between diluted (2:3) hydrochloric acid and a weighted amount of powdered rock as a function of temperature and pressure is produced. The chemical reaction releases CO_2 that is acting a pressure on a graduated burette filled by MilliQ water. The higher the water displaced the higher the content of $CaCO_3$, according to the following equation:

$$\mathrm{CaCO_3wt\%} = (x + \mathrm{h})\,/2$$

where x is the level of water displaced and h is a correction factor due to the adsorption of the hydrochloric solution during the above-mentioned reaction.

Portable X-Ray Fluorescence (pXRF)

The portable Elio (Bruker, Berlin, Germany) instrument, equipped with a rhodium anode X-ray source (voltage < 50 kV, current < 0.2 mA, collimation diameter: 1 mm), and a Silicon Drift Detector (SDD) with an active area of 50 mm^2 and a resolution of < 140 eV for the Mn Kα line, with an energy range from 1 to 40 keV, was used to obtain semi-quantitative composition of the different coloured areas and maps (Santo et al., 2025 for details). The distance between the object and the detector is approximately 7 mm, and the distance between the object and the front of the instrument is approximately 10 mm. Spot analyses were conducted at 50 kV and 80 µA for at least 120 s. The same kV and µA conditions were applied for mapping.

Electron Microprobe (EPM)

Minerals present in representative pebbles were analysed through a Jeol JXA-8230 Electron Microprobe at 15 kV

accelerating voltage and 20 nA beam current, using 15 s counting times on peaks (and for both backgrounds) for major elements; times were increased to 40 s for oxides in <1 wt% amounts. Wavelength-dispersive spectroscopy (WDS) maps were performed at 15 kV and 50 nA, using 0.20 mm size and 20 msec dwell time.

Raman Spectroscopy

Micro-Raman analyses of the sample surfaces were performed by means of a Renishaw RM2000 with 785 nm diode laser as excitation line. The laser power on the analysed samples was adjusted between 0.2 and 1 mW, to avoid potential laser-induced modifications. Microscope objectives of different magnification (20x, 50x) were used to preliminarily observe the morphology of the samples by white light, while spectra were acquired using a 50x (N.A. = 0.75) magnification objective, providing a spot size of approximately 2 µm. The spectral range investigated was between 200 and 1800 cm^{-1}, with a spectral resolution of 4 cm^{-1}, and the acquisition times between 10 s and 30 s. Three acquisitions per spot were made and averaged to improve the signal to noise ratio. Raman spectra are analysed by first removing the background using a polynomial function and then fitting the resulting peaks in the spectral range 200–700 cm^{-1} with Gaussian functions, to extract peak positions, intensities, and widths.

Results

The use of different analytical techniques made it possible to obtain the results reported below.

Optical Microscopy

The most striking feature of rocks is the vivid banding of colours, from orange-red, golden yellow, to brown and grey/black tones (Fig. 5a-c). Additionally, a complex network of stylolitic joints and veins characterizes the rock. These veins, mainly composed of calcites and minor quartz, crosscut the rock in multiple orientations, displacing colour bands and producing striking textural and chromatic effects of great beauty and interest (e.g. Figure 5a, b). Their dimensions vary, ranging from microveins to veins several hundred microns wide. The calcite crystals in the veins can exceed 400 microns in size, while the quartz crystals are generally smaller, ranging from 100 to 150 microns (Fig. 5f). The samples are fine to very fine-grained rocks, with a clay-dominated matrix and subordinate carbonate content. Dispersed throughout the matrix, which looks dense and homogeneous are small quartz crystals (50–150 µm - Fig. 5d), with rare muscovite and iron/manganese oxides, the latter occasionally forming dendritic patterns (Fig. 5e). The fine grain size and diagenetic overprint make detailed classification challenging, though the rock can broadly be identified as a diagenetically altered mudrock with evidence of pressure solution and fluid-driven mineralization.

X-Ray Powder Diffraction (XRDP)

Several selected pebbles were analysed both as whole rocks and as separate powders from differently coloured areas (red, yellow, and grey). The mineralogical data reported in Table 1 for the whole rock and coloured portions represent the average results obtained from ten different specimens. They indicate that the rock consists of quartz (qz), calcite (cc), phyllosilicates (primarily kaolinite), and low amounts of hematite and goethite. In particular, hematite and goethite were detected in the red areas (Table 1; Fig. 6), whereas only goethite was found in the yellow areas. In the grey areas, quartz, calcite, feldspar (albite) and phyllosilicates (kaolinite, illite and muscovite) were detected. The presence of kaolinite may indicate extensive chemical alteration, further supported by the detection of goethite and hematite, which are typical iron-bearing weathering products.

Calcimetry

For the determination of calcium carbonate ($CaCO_3$) on the whole rock, we selected three pebbles (M9AGa, M9AGb, CT2013). For each sample, the analyses were repeated three times (Table S1). The determination of calcium carbonate ($CaCO_3$) is slightly variable from 20.0 to 21.0 wt% (average: 20.3 wt%) in the analysed samples.

Table 1 Qualitative mineralogical composition (mean), obtained by XRDP analyses, of the whole rock and separate powders from differently coloured areas of the studied pebbles

Sample	Quartz	Calcite	Phyllosilicates	Hematite	Goethite	Feldspar
Whole rock	x	x	x (kaolinite)	tr	tr	nd
Red	x	x	x (kaolinite)	tr	tr	nd
Yellow	x	x	x (kaolinite)	nd	tr	nd
Grey	x	x	x (kaolinite, illite, muscovite)	nd	nd	x (albite)

x detected, *tr* trace amounts, *nd* not detected

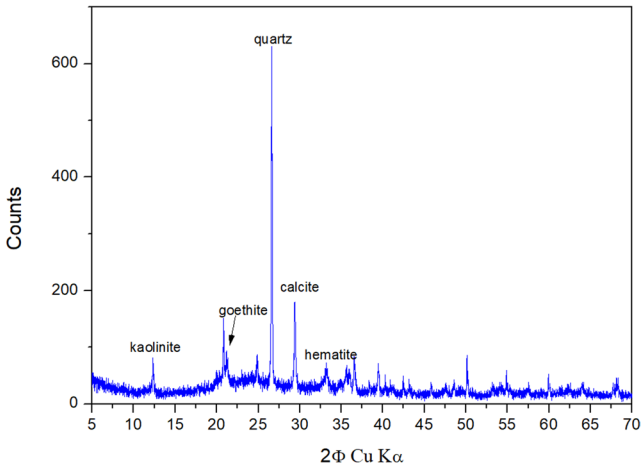

Fig. 6 Representative XRDP spectrum of a red portion of *giottoli*. The most intense peaks of each detected phase are reported

Portable X-Ray Fluorescence (pXRF)

Selected *giottoli* were investigated using portable X-ray fluorescence. Spot analyses and compositional maps were carried out on areas showing different colours.Table S2 shows, as example, the intensities obtained by XRF, at six different points on the sample M9AGb (Fig. 7b). The intensities are reported for the area, background, and peak of each element. Concerning the different spot analyses, it was possible to observe that Silicon (Si), Aluminum (Al), and Iron (Fe) show the greatest variability across the analysed points, suggesting significant differences in mineral compositions or the activation of different geological processes across samples. The range of calcium (Ca) content is not as wide as Si or Al, but still shows some significant variation. Titanium (Ti) and Manganese (Mn) exhibit relatively small variations, with Ti remaining nearly constant in most samples, and Mn showing trace or low values in all but one sample. Overall, Si and Ca appear to be dominant elements, with Fe also showing significant variability. The higher variability in elements like Al and Fe might also suggest varying mineralization patterns.

The composition obtained through spot pXRF analyses, although only semi-quantitative, allowed us to estimate the percentages of the minerals present in the studied pebble using a simplified normative mineralogy approach (a modified CIPW norm, adapted for weathered or sedimentary materials, given the presence of kaolinite and goethite identified by XRDP. Spot pXRF oxide totals were normalized to

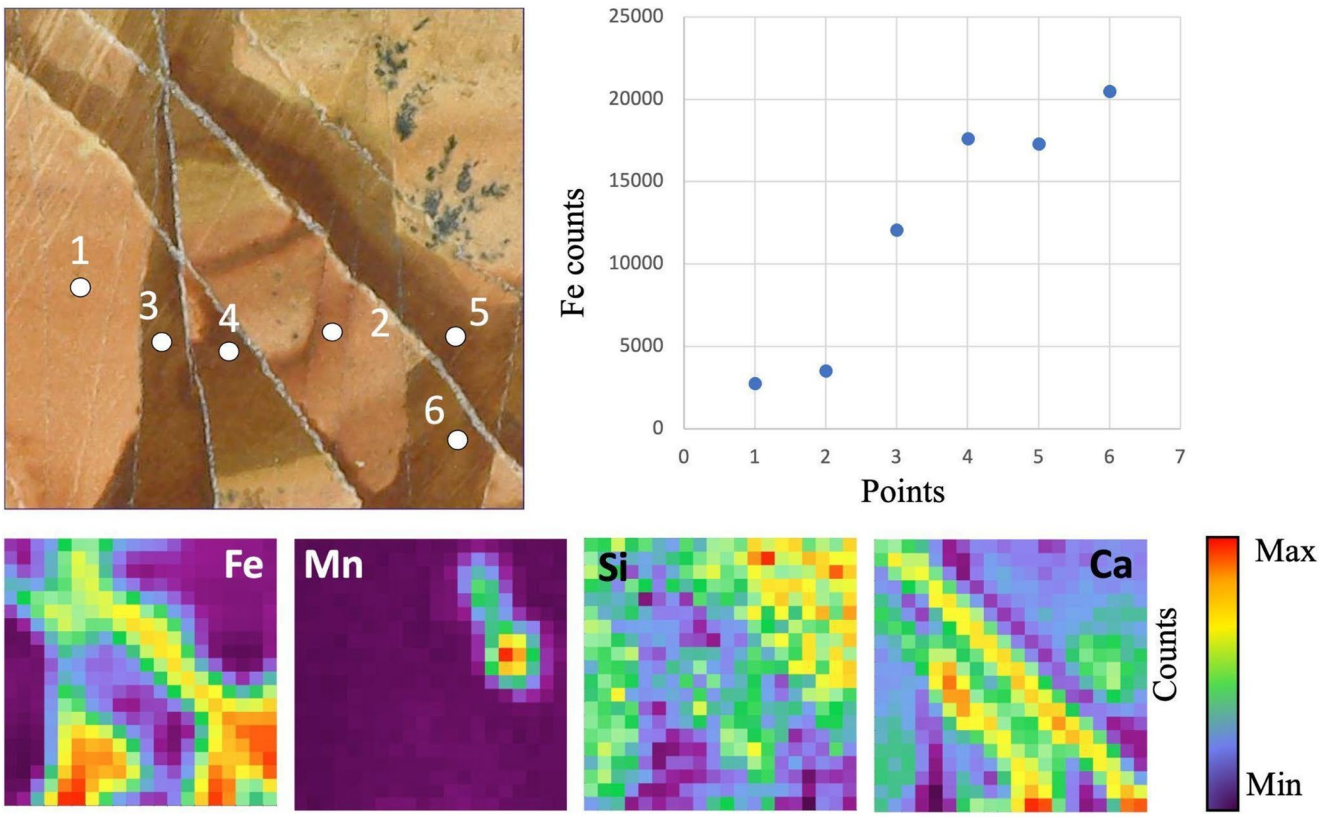

Fig. 7 Top left: Optical image of one of the analysed areas (2 cm × 2 cm) in the sample M9AGb, with annotated analytical points; top right: Fe count graph showing the corresponding XRF-derived iron signal at each marked point. Different intensities of red colour in the optical image reflect variations in iron content. Elemental distribution maps obtained in the same area for Fe, Mn, Si, and Ca are shown at the bottom

100% (anhydrous), secondary phases identified by XRDP (kaolinite and iron oxyhydroxides) were accounted for by subtracting their stoichiometric oxide equivalents prior to the normative calculations, and different Fe^{2+}/Fe^{3+} partitioning scenarios were tested to assess uncertainty. The resulting normative mineral fractions were then reconstituted into modal percentages. This approach follows established adaptations of CIPW for weathered and sedimentary materials and provides first-order modal estimates which are discussed together with their limitations (Cross et al., 1902/1903; Cohen and Ward 1991; Voicu et al., 1997). Accordingly, we obtained the following approximate percentage: quartz 50%, kaolinite 25%, calcite 20%, iron oxyhydroxides 5%. These percentages are in good agreement with the optical observation and the calcimetry results. Figure 7 displays a selected area of one of the studied pebbles, M9AGb, together with its corresponding elemental distribution maps and FeO counts at various marked points in the red area. The compositional map provides clear evidence of significant chemical heterogeneity within the analysed pebble. Iron distribution is particularly variable, with higher concentrations aligning closely with the darker areas of the pebble, indicating a strong correlation between iron enrichment and visual appearance. This is especially apparent in the Fe map and is quantitatively supported by the Fe count plot, which shows a wide range of values across the sampled points. Manganese is notably confined to a small, well-defined area in the upper right, coinciding with the dendritic structures visible in the optical image. This suggests localised Mn enrichment, likely linked to specific microstructural features. Calcium is concentrated along distinct vein-like structures cutting across the sample, implying a secondary mineralisation process or fluid-driven alteration that enriched Ca in these linear zones. In contrast, silicon shows an inverse relationship with iron, being more abundant in Fe-poor areas, which highlights clear compositional zoning within the pebble. Overall, the elemental distribution maps, combined with the Fe count plot, reveal a complex interplay of mineral phases and suggest multiple processes, including fluid infiltration and localised crystallisation, contributing to the observed heterogeneity. Furthermore, it is important to consider that the pXRF beam has a diameter of approximately 1 mm, whereas the compositional zoning within the pebbles may occur also at sub-millimetric scales. Consequently, the X-ray beam may, in some cases, interact with a compositionally heterogeneous area, potentially affecting the accuracy of the measurements.

Electron Microprobe (EPM)

Scanned thin-section images of three representative samples (M9AGb, M9AGa, CT2013b) are shown in Fig. 8. From these images, a total of eight small areas (highlighted in red, yellow, and grey) were selected for b*ackscattered electron* (BSE) imaging and electron probe microanalysis (EPMA).

An example of a BSE image, from site 1 of M9AGb sample (Fig. 8a) is shown in Fig. 9. In particular, taking into consideration the sample CT2013b, three areas displaying distinct colours (red, yellow, and grey) were selected for WDS mapping (Fig. 10). BSE imaging revealed the presence of several distinct phases (discussed later), including a dispersed Al-rich silicate phase—almost certainly

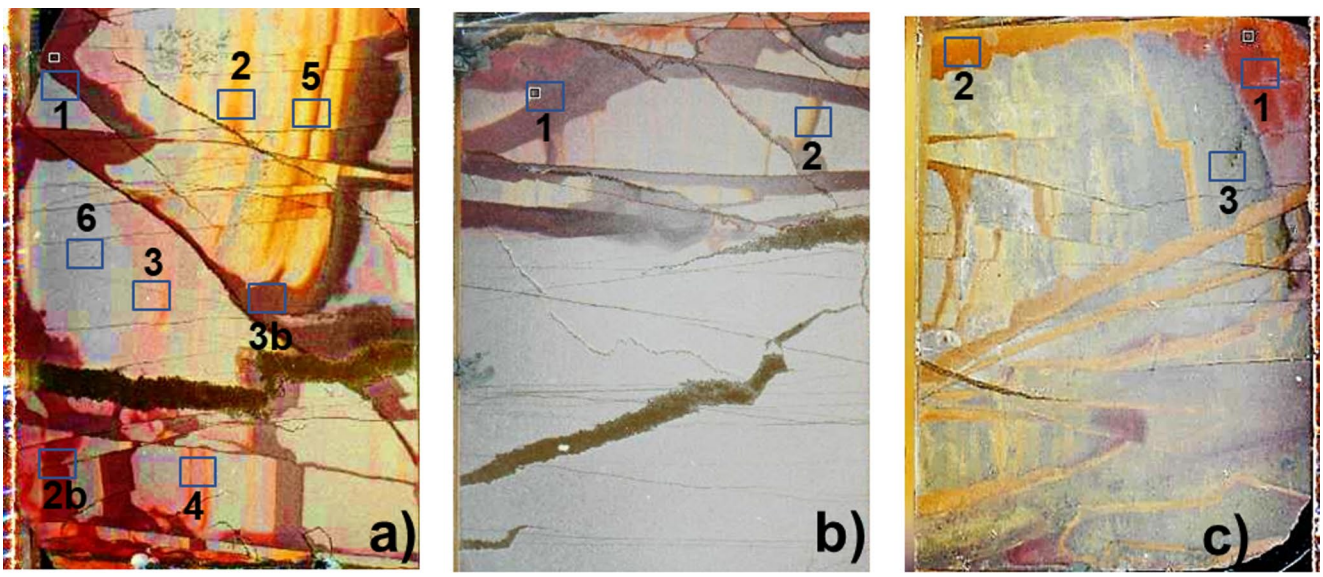

Fig. 8 Scanned thin section images of analysed pebbles with reported sites of EPM analyses and maps. **a)** sample M9AGb: 1, 2b, 3, 3b, 4 = red areas, 2, 5 = yellow areas, 6 = grey area; **b)** Sample M9AGa: 1 = red area, 2 = yellow area; **c**) Sample CT2013b: 1 = red area, 2 = yellow area, 3 = grey area

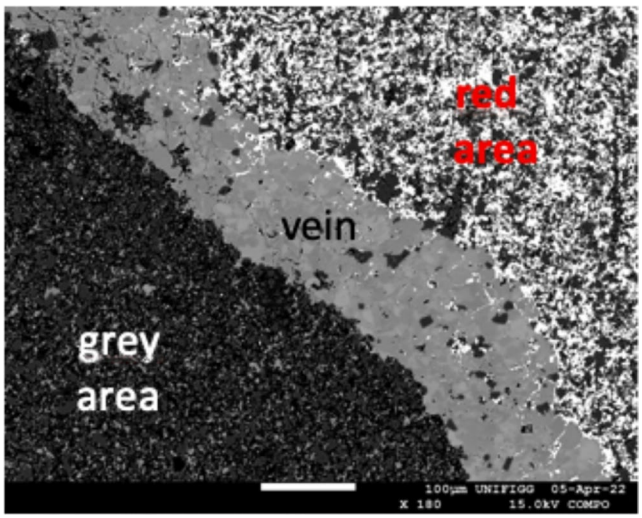

Fig. 9 BSE image of site 1 (see M9AGb sample, Fig. 8a). The site is across grey and red areas and is separated by a carbonatic vein. The length of the bar is 100 µm

kaolinite, as identified by XRDP analysis. However, due to its extremely fine (<5 µm) grain size, this phase could not be analysed with this technique. Similarly, the presence of minor organic matter, possibly scattered within pebbles and also not analysable, cannot be ruled out. Consequently, our analyses focused on the remaining phases.

Combined BSE imaging and WDS analyses (Figs. 9 and 10, Table S3) provided the following insights:

Grey areas - These are mainly composed of quartz, with a minor amount of calcite, typically less than 50 µm in size (Fig. 9). Calcite contains low quantities of MgO (0.4–1.1 wt%), MnO (up to 1 wt%), and FeO (~0.03 wt%). Rare FeOx are also observed. Since these crystals rarely exceed 3 µm, accurate analysis is challenging, and careful selection of measurement points is essential.
Red and yellow areas - The red areas consist of intergrowths of quartz, calcite, and FeOx with sizes up to 5 µm (Fig. 9). The qz and cc grain sizes are similar to those in grey areas. The composition of FeOx is comparable to that in the grey areas, but their modal abundance is significantly higher, similar to that of qz and cc, as shown in the WDS maps, relative to CT2013b sample (Fig. 10). The only notable difference between coloured and grey areas is evident in the iron map, where variations in intensity correspond to differences in the modal amount of FeOx phase. No noticeable difference in FeOx abundance was observed between red and yellow areas in the analysed samples.
Veins - These are mostly composed of cc, with a minor amount of qz and FeOx (Fig. 9). The composition of the veins is heterogeneous, as nearly pure calcites coexist with calcite containing FeO (up to ~0.8 wt%), MnO (up to ~0.5 wt%), and MgO (up to ~0.3 wt%).

Electron microprobe analyses (expressed as oxides) of Fe-rich phases in the yellow and red areas revealed that, in addition to the dominant FeO content (60–78 wt%, Fig. 11), the samples also contain SiO_2 (3–11 wt%), CaO (up to 4.5 wt%), Al_2O_3 (0.5–6.5 wt%), MnO (up to 0.35 wt%), and MgO (up to 0.55 wt%). While some contamination from quartz, calcite, and clay minerals during analysis cannot be completely excluded, we are confident that these elements are present in the FeOx phase, particularly SiO_2, which consistently falls within the 4–7 wt% range (Table S3, Fig. 11a). Analyses of the red and yellow areas (Table S3) show no significant chemical differences between them. However, measurements from yellow areas generally exhibit slightly higher MnO and MgO contents than those from red areas. Calcite analyses from both red and yellow areas indicate that cc in the yellow areas tends to be richer in MnO (0.3–0.5 wt%, Fig. 11f) compared to cc in red areas, which generally contains less than 0.15 wt% MnO (Table S4 Fig. 11f).

Raman Spectroscopy

The thin section M9AGb previously analysed by EPM across its red, yellow, and grey areas, was also examined using micro-Raman spectroscopy. Additional spectra acquired directly on the uncoated coloured sample confirmed the same mineralogical features observed in the thin section. Figure 12 shows representative Raman spectra collected from different sites of the sample.

The Raman spectra on the grey area (site 6 in Fig. 8a) display strong α-quartz fingerprint bands, with peaks at 464 cm^{-1} (Si–O–Si symmetric stretching) and 206 cm^{-1} (lattice vibrations). Additional broad and weak bands are visible at ~390 cm^{-1} (lattice modes) and 805 cm^{-1} (Si–O–Si bending). Peaks at 642 cm^{-1} and 1080 cm^{-1} are attributed to symmetric and asymmetric Si–O–Si stretching vibrations, likely related to phyllosilicates (Fig. 12a; Wang 2015). The Raman spectra of the yellow areas (sites 2 and 5 in Fig. 8a) are characterised by a sharp band at 303 cm^{-1}, a broad band at 394 cm^{-1}, and three additional weaker bands at 250, 484, and 558 cm^{-1}. These occur alongside a strong ~464 cm^{-1} quartz peak and a distinct ~1085 cm^{-1} band corresponding to the ν_1 symmetric stretching mode of calcite. (Fig. 12b). These latter vibrational modes are also visible in Fig. 12c, which presents Raman spectra acquired from four reddish areas (sites 1, 2b, 3b, and 4 in Fig. 8a). Diagnostic bands at 225, 296, 410, 612 cm^{-1} indicate the presence of hematite; however, the observed band broadening, spectral asymmetry, and the additional band at ~557 cm^{-1} suggest a mixture

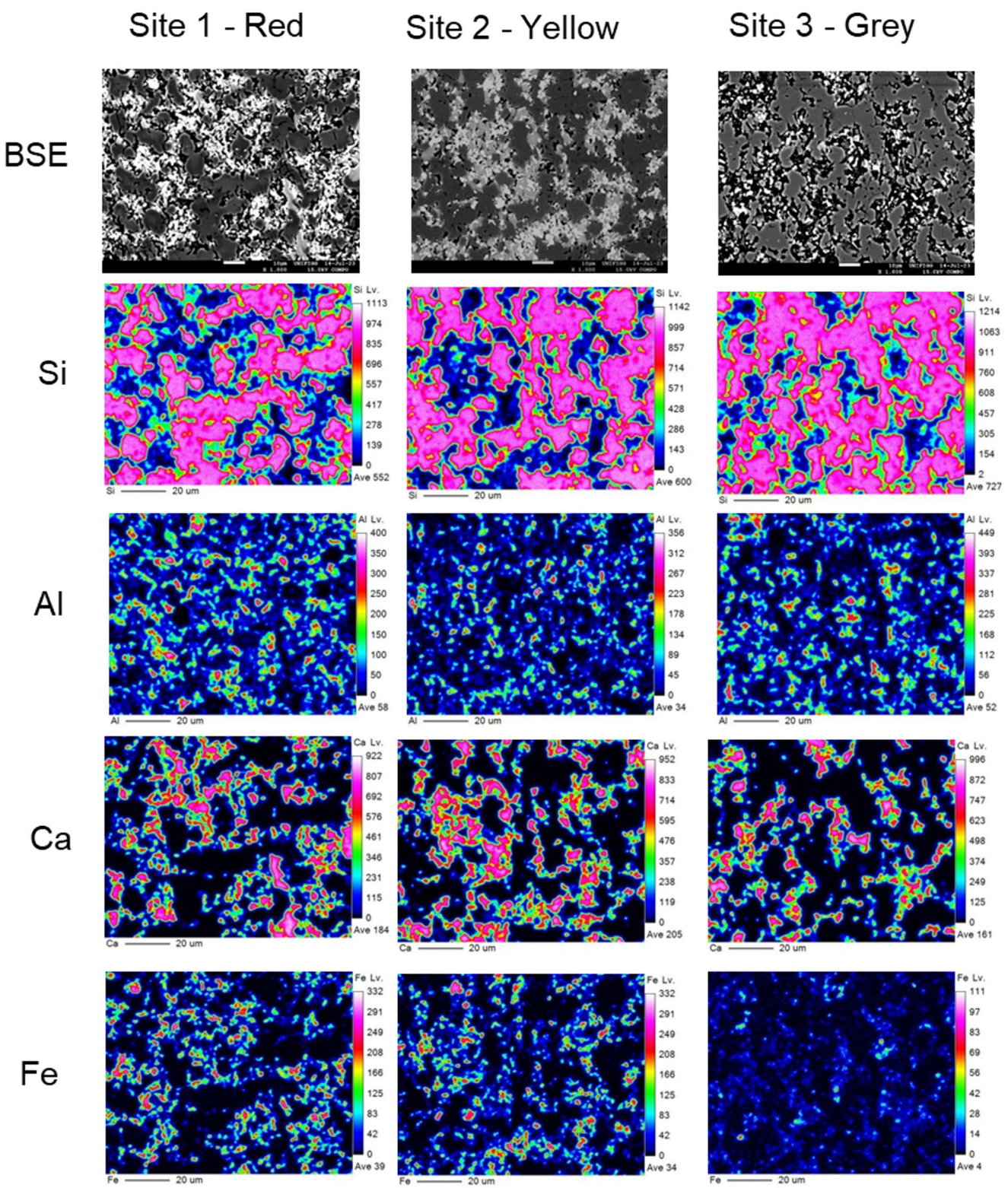

Fig. 10 Backscattered electron images of the studied areas (red, yellow, grey) and corresponding WDS elemental maps in sites 1,2,3 of CT2013b sample (see Fig. 8c). Colour scale indicates the intensity of Si, Al, Ca, Fe Kα lines

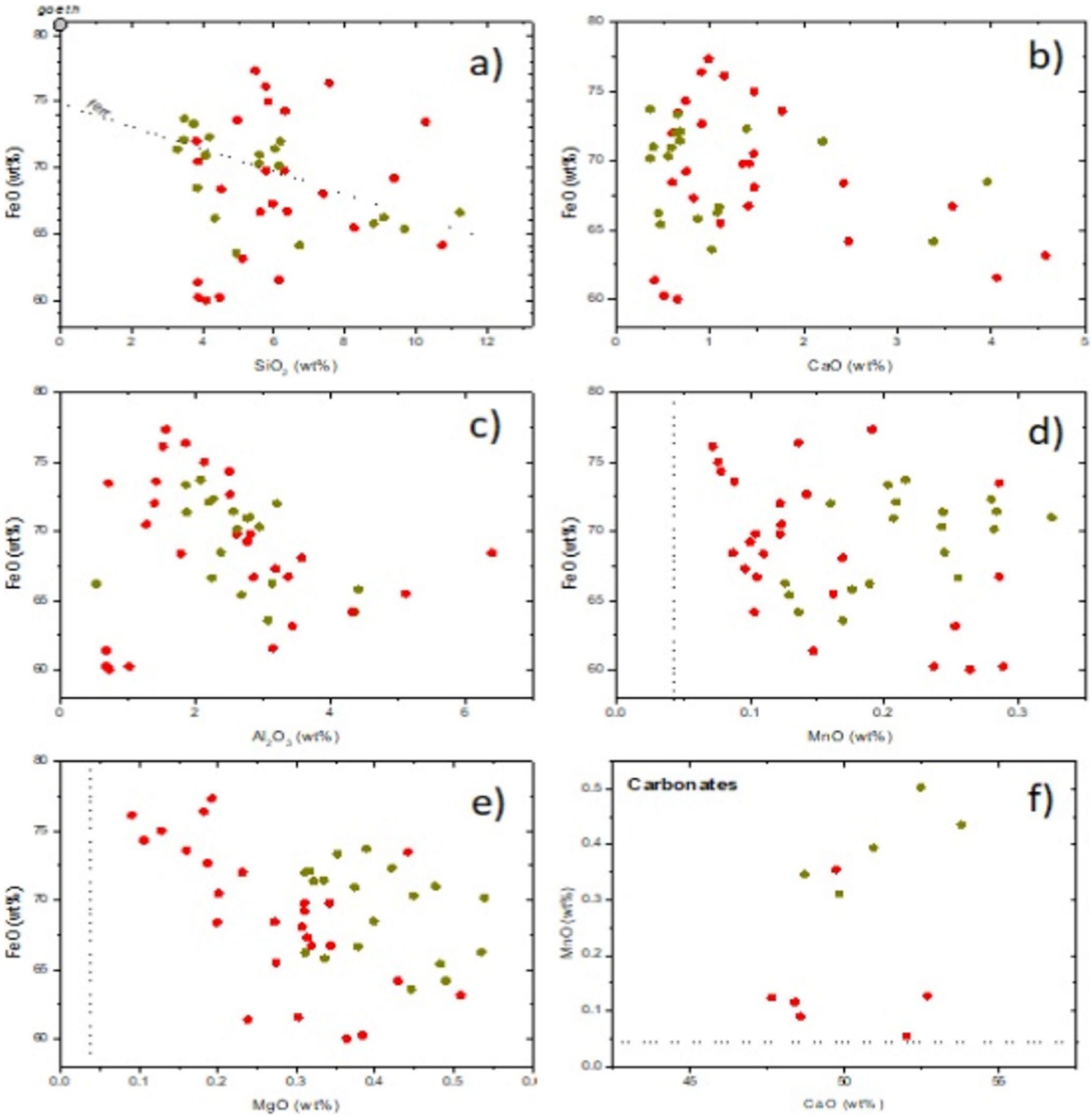

Fig. 11 a-e) FeO vs. SiO_2, CaO, Al_2O_3, MnO, and MgO in FeOx in red (red symbols) and yellow (green circles) areas. Dot line in FeO vs. SiO_2 graph represents the connection line between Si-free ferrihydrite and Si-rich ferrihydrite. Goeth (grey circle in Fig. 11a): composition of goethite. The dotted line in a) indicates a Si-free to Si-rich end-member trend proposed by Evans et al., (2021). Dot lines in MnO and MgO graphs represent detection limits; f) MnO vs. CaO in calcite in coloured areas

of iron oxide and hydroxide phases. Gaussian peak fitting further reveals the coexistence of vibrational modes attributable to hematite and components typical of the yellow areas' spectra. The dark red colour observed macroscopically likely corresponds to hematite enrichment. In Fig. 13a, we report the fitting Raman spectra from the red sites, highlighting the characteristic hematite frequencies as well as the vibrational features observed in the yellow areas. Variations in bandwidth and intensity among the different areas analysed suggest differences in crystallinity, elemental substitution (e.g., Al for Fe), and particle size among the iron-bearing phases.

Raman spectra collected from the yellow areas (sites 2 and 5) exhibit bands consistent with goethite but show

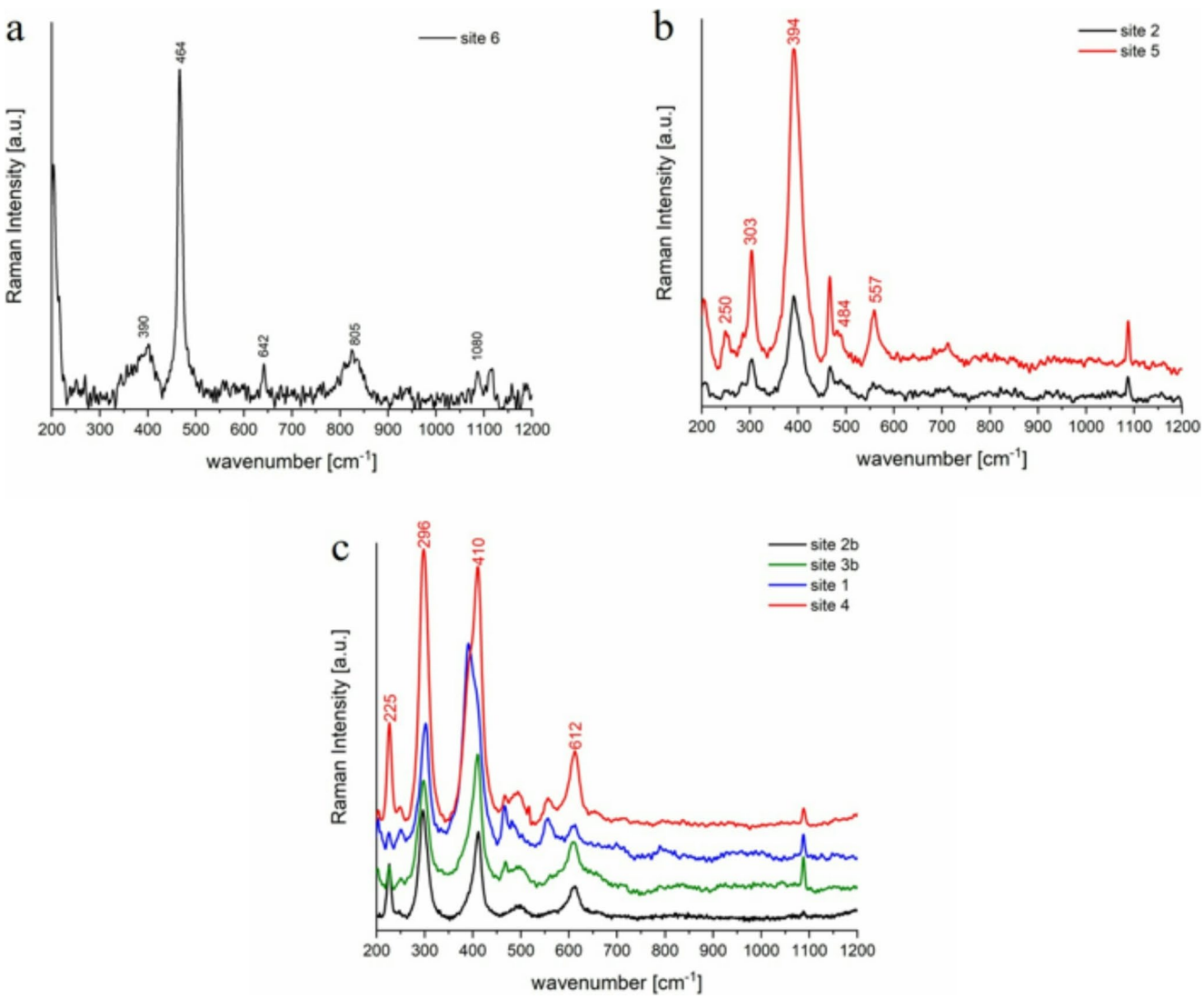

Fig. 12 Baseline-corrected Raman spectra acquired from thin section M9AGb: **a)** grey site — dominant α-quartz peaks (~206, 464 cm^{-1}); **b)** yellow sites — goethite-related bands (~303, 394 cm^{-1}) with quartz and calcite; **c)** red sites — hematite features (~225, 296, 410, 612 cm^{-1}) and coexisting hydroxide bands

notable differences in peak positions and widths compared to the RRUFF natural goethite reference spectrum (Fig. 13b). In particular, a systematic shift to higher wavenumbers, accompanied by moderate broadening in the 300–600 cm^{-1} region, suggests the presence of Al-substituted goethite (Liu 2013). The ionic radius of Al^{3+} (0.53 Å) is slightly smaller than that of Fe^{3+} (0.65 Å); thus, Al-for-Fe substitution shortens bond lengths and increases bonding force, leading to shifts toward higher wavenumbers. Based on comparison with Liu's experimental data, the observed shifts suggest an Al content of approximately 9–10% in the goethite lattice. In hydrothermal environments where hematite and goethite coexist, Al^{3+} preferentially incorporates into goethite due to its greater structural flexibility. Density Functional Theory (DFT) simulations confirm this substitution is thermodynamically favoured, with lower energetic barriers than in hematite (Guimarães et al., 2023). Moreover, Al substitution stabilizes the goethite lattice by reducing lattice strain and strengthening Fe–O bond networks, which slows the transformation to hematite under hydrothermal conditions. (Cornell and Schwertmann 2003; Liu et al., 2013; Guimarães et al., 2023). The presence of other iron hydroxides commonly formed under hydrothermal conditions, such as ferrihydrite and akaganeite (β-FeOOH), cannot be completely excluded. Akaganeite exhibits Raman bands that significantly overlap with those of Al-substituted goethite, especially in the 300–400 cm^{-1} region, complicating precise phase identification. Ferrihydrite, a poorly crystalline iron hydroxide, typically exhibits broad and weak Raman bands centered at approximately 370, 510, and 710 cm^{-1} (Mazzetti

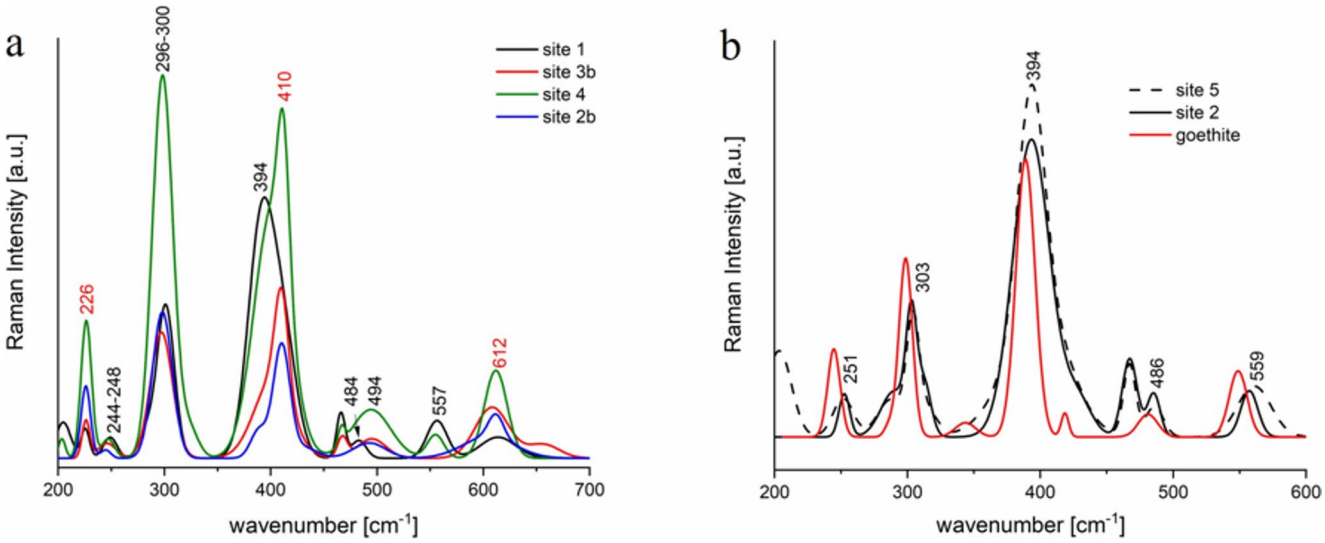

Fig. 13 **a)** Gaussian peak fitting of baseline-corrected Raman spectra from the red areas (sites 1,2b,3b,4 in Fig. 8a). Characteristic hematite bands are marked in red, while coexisting vibrational features consistent with goethite or Al-substituted goethite are marked in black. **b)** Gaussian fitting of baseline-corrected Raman spectra from the yellow areas (sites 2 and 5 in Fig. 8a). Peak positions associated with Al-substituted goethite are shown in black. For comparison, the Raman spectrum of natural goethite from the RRUFF database is overlaid in red

2002). Among these, the ~710 cm^{-1} band is particularly difficult to isolate in the present spectra, as it overlaps with the ν_4 vibration of calcite at ~712 cm^{-1}, complicating detection. Furthermore, ferrihydrite may undergo laser-induced transformation into hematite, even at low excitation powers typically used in microRaman spectroscopy. These factors hinder unambiguous identification. Furthermore, differences in Raman band intensities, despite consistent peak positions, suggest that the analysed areas consist of nanocrystalline aggregates. These variations are attributed to orientation-dependent scattering and partial depolarization effects, which are typical in Raman spectra of randomly oriented crystallites within the laser spot (~2 μm) Faria et al., 1997).

The co-occurrence of Fe oxyhydroxides, silicate, and carbonate bands suggests a multiphase assemblage typical of hydrothermal systems, potentially reflecting redox gradients and fluid evolution.

Discussion

This study focused on *giottoli*, distinctive pebbles from Southern Tuscany that exhibit vivid, naturally occurring colour patterns reminiscent of abstract art. Superficially, they resemble *Pietra Paesina*, a marly limestone from Central Italy whose origin remains debated. Pietra Paesina's characteristic banding has been attributed to periodic precipitation of iron hydroxides, either during diagenesis or more likely through weathering processes (Serra et al., 2010). While *giottoli* share some aesthetic features, they differ significantly in their broader colour spectrum and more abstract patterns, distinguishing them from traditional ornamental stones.

Despite their uniqueness, *giottoli* have received little scientific attention, with only a few studies (Mari 2018; Mougenot and Mari 2021) and one exhibition ("Giottolandia", Museum of Natural History, Florence, 2018) addressing them. Mougenot and Mari (2021) suggested that *giottoli* encapsulate the complex geological history of Tuscany, from Cretaceous sedimentation through the Apennine orogeny, magmatic activity, weathering, and erosion, culminating in their deposition along rivers and beaches. As such, they serve as natural archives of regional tectonic and hydrothermal evolution, expressed through their unique mineralogy and chromatic features.

Colour Variability in *Giottoli*

The most striking feature of *giottoli* is their rich colour palette, which immediately attracted our attention. Composed mainly of quartz, calcite, Fe-rich phases, clay minerals, and possibly organic matter, their colours reflect variations in mineral content and their composition. Among these, FeOx are the primary contributors to colour variability, as confirmed by XRF, EPMA, XRDP, and Raman analyses.

FeOx phases are abundant in red and yellow areas and nearly absent in grey zones. However, due to their fine grain size (<3 μm) and complex chemistry, often incorporating Si, Al, Ca, Mn, and Mg, identifying these phases is challenging.

XRDP and Raman data suggest that yellow zones are dominated by goethite (FeO(OH)), while red zones contain both goethite and hematite (Fe_2O_3). Amorphous FeOx phases such as ferrihydrite ($2.5Fe_2O_3 \cdot 4.5\ H_2O$) may also be present, although undetectable via XRDP and not completely excluded by Raman data.

Ferrihydrite, typically forming nanocrystals with high surface areas ($2–4 \times 10^5$ m^2/kg; Schwertmann and Taylor 1989), is known to incorporate Si, Al, and Mn (Childs 1992; Cismasu et al., 2011; Manceau and Gates 2013), as supported by our EMP analyses. In particular, a Si-free to Si-rich end-member trend (Fig. 11a) was proposed by Evans et al., (2021), acknowledging that Si may be adsorbed rather than structurally bound. This variability likely contributes to the broad range of FeO contents (60–77 wt%, Fig. 11) and may explain the compositional scatter observed in our microanalyses. The presence of organic matter, often coexisting with ferrihydrite (Thomas Arrigo et al., 2020; Zhao et al., 2022), could further influence the mineralogy and colour.

Ferrihydrite's hue, ranging from 7.5 yellow-red (YR) to 2.5 YR, is affected by crystal size, cementation, and elemental substitutions (Schwertmann 1993). While our data do not definitively confirm this, variations in Si content might impact brightness and tone. Ferrihydrite can adsorb Mn(II) and incorporate Al depending on precipitation conditions (Lan et al., 2021; Vodyanitskii and Shoba 2016), further complicating its spectral signature. Though XRDP and Raman failed to identify it due to poor crystallinity, its presence cannot be excluded.

Notably, Mn concentrations are higher in FeOx phases within yellow zones (Fig. 11d), a trend that becomes more evident when examining the chemistry of associated calcite (Fig. 11f). This suggests that colour variations may also be influenced by carbonate composition. The role of Mn and other cations in modulating FeOx colour, particularly in goethite and ferrihydrite, has been documented (Cornell and Schwertmann 2003) and aligns with our findings.

How Might *Giottoli* Have Formed?

The association between Ca-rich veins and coloured bands (Figs. 8 and 9) suggests that colour development in *giottoli* may involve rhythmic precipitation processes, akin to Liesegang banding. Such features, commonly seen in "zebra rocks," record non-equilibrium fluid-rock interactions involving supersaturation, diffusion, nucleation, and chemical reactions (Ortoleva 1984, 1993; Sadek and Sultan 2010; Yoshida et al., 2020). In these systems, Fe-rich fluids migrate through microfractures and porosity, precipitating iron oxyhydroxides as redox or pH conditions change, typically due to buffering with host minerals. For example, Yoshida et al., (2020) showed how Fe(III)-rich fluids, interacting with dacitic cobbles, precipitate iron phases as pH rises due to plagioclase alteration. Band thickness reflects the duration of each reaction-diffusion cycle, a kind of geochemical "fossil" of fluid-rock interaction. Coward et al., (2023) observed similar features in East Kimberley's zebra rocks, linking hematite banding to Fe(II) oxidation during acidic fluid infiltration. Band formation ceased with Fe(II)/oxidant depletion or fluid neutralisation. They also suggested that Ostwald ripening may play a role in the post-precipitation evolution of Fe oxides. Similarly, Kawahara et al., (2022) proposed that Fe oxide bands form when acidic fluids, enriched in Fe and derived from pyrite-bearing rocks, react with calcite, causing pH fluctuations and stepwise Fe-oxide precipitation. *Giottoli* display comparable textures, fine-grained sedimentary matrices with stylolites and mineralised veins. The rocks are matrix-supported with dispersed quartz and muscovite grains, and show clear evidence of post-compaction fluid movement and multiple diagenetic events. Veins filled with calcite and quartz, dendritic oxide textures, and chromatic banding point to a complex alteration history. These rocks can be classified as siliciclastic mudstones with significant diagenetic overprints. We hypothesise the following sequence: (1) sedimentation of clay and detrital grains, (2) compaction and stylolite formation, (3) fluid migration depositing cc and qz, (4) iron-rich fluids interacting with calcite veins, causing pH variations and rhythmic Fe-oxide precipitation. This model closely aligns with findings in the Colline Metallifere region of Tuscany, where pyrite- and chalcopyrite-rich deposits have produced acid mine drainage upon weathering. These acidic fluids, enriched in Fe^{2+}, were oxidised and hydrolysed during interaction with carbonate veins, resulting in FeOx precipitation with characteristic colour banding.

In this study, we focused on the analysis of *giottoli* that predominantly display red, yellow, and grey hues. These colours likely result from distinctive mineralogical compositions and geochemical processes that occurred during the diagenetic or post-diagenetic stages of rock formation.

Nevertheless, *giottoli* are far from uniform in appearance; they exhibit a striking chromatic diversity (Fig. 1), with some specimens presenting less common yet vivid colours such as green, blue, and purple. Drawing analogies with the findings obtained from our analysis, it is plausible to propose that these additional colourations may arise from the same fundamental set of geochemical processes. The chromatic variability observed is likely regulated by the concentration and oxidation state of specific chemical elements. Iron (Fe) and manganese (Mn) play a dominant role in this process, with their valence states and mineral associations contributing significantly to the resulting colours. However, we cannot exclude the presence of elements with

known chromophore properties, including copper, chromium, and cobalt, which may further enhance or alter the colouration patterns through complex substitution mechanisms or secondary mineral formations.

The understanding of these processes not only sheds light on the origin of colour in *giottoli*, but also opens new avenues for interpreting the geological and geochemical history of the regions from which they were sourced. As such, the systematic study of *giottoli* exhibiting a wider range of colours promises to be a rich and rewarding subject for future research, offering new insights into fluid-rock interaction processes and trace element geochemistry in sedimentary environments.

Conclusions

Giottoli are siliciclastic mudstones containing approximately 20 wt% of calcite. Their most striking feature is the colour variability, with predominant red and yellow areas of varying intensities superimposed on a grey matrix primarily composed of quartz, calcite, and kaolinite. Calcite veins almost always delineate the coloured zones, suggesting they play a role in controlling colour development. Goethite and Al substituted goethite (in both red and yellow areas), hematite (exclusively in red areas), and possibly ferrihydrite are the phases responsible for the observed colours. These Fe oxyhydroxides incorporate varying amounts of Si, Al, Ca, Mg, and Mn. Among these elements, manganese appears to influence colour the most: MnO concentrations in FeOx typically exceed 0.15 wt% in yellow areas but fall below this threshold in red areas. *Giottoli* are found in river basins draining the Colline Metallifere region, which may have provided the iron now present as FeOx. Mine tailings in this area often contain Fe-sulphides (e.g., pyrite), which oxidize to produce acid mine drainage. This process releases Fe^{2+} into solution and lowers pH. As acidic, Fe-rich solutions percolate through the pebbles, FeOx precipitate upon pH neutralization, primarily driven by interactions with carbonate minerals hosted in veins crosscutting the pebbles. In this context, *giottoli* could be interpreted as a natural example of "zebra rocks," where Liesegang-type rhythmic patterns result from fluid–rock interactions.

The research demonstrates how personal fascination can catalyse scientific investigation. The analysis of these *giottoli* not only provided new insights into sedimentary and mineralogical processes but also highlighted the value of accessible, relatable science. By acknowledging and fostering public engagement, geoscientists can shift perceptions, promote scientific literacy, and reaffirm the relevance of geology in addressing contemporary environmental and societal challenges.

Supplementary Information The online version contains supplementary material available at https://doi.org/10.1007/s12371-025-01233-y.

Acknowledgements The authors would like to express their gratitude to Eleonora Braschi and Sara Calandra for their help during EPM and XRF analyses, respectively.

Authors' Contributions A.O., M.G.B., E.P., M.R., A.P.S - Conceptualization, Methodology, Sample Analysis, Writing-Review and editing.

Funding Open access funding provided by Università degli Studi di Firenze within the CRUI-CARE Agreement. This research did not receive any specific grant from funding agencies in public, commercial, or not-for-profit sectors.

Data Availability The datasets analyzed during the current study are available from the corresponding author upon reasonable request.

Declarations

Competing interests The authors declare no competing interests.

References

Bonini M, Sani F, Stucchi EM, Moratti G, Benvenuti M, Menanno G, Tanini C (2014) Late Miocene shortening of the Northern Apennines back-arc. J Geodyn 74:1–31. https://doi.org/10.1016/j.jog.2013.11.002

Childs CW (1992) Ferrihydrite: a review of structure, properties and occurrence in relation to soils. J Plant Nutr Soil Sci 155(5):441–448. https://doi.org/10.1002/jpln.19921550515

Cismasu AC, Michel FM, Tcaciuc AP, Tyliszczak T, Brown GE Jr (2011) Composition and structural aspects of naturally occurring ferrihydrite. CR Geosci 343(2–3):210–218. https://doi.org/10.1016/j.crte.2010.11.001

Cohen D, Ward CR (1991) Sednorm — a program to calculate a normative mineralogy for sedimentary rocks based on chemical analyses. Comput Geosci 17:1235–1253

Conti P, Cornamusini G, Carmignani L (2020) An outline of the geology of the Northern Apennines (Italy), with geological map at 1:250,000 scale. Ital J Geosci 139:149–194

Cornell RM, Schwertmann U (2003) The iron oxides: structure, properties, reactions, occurrences, and uses. Wiley-VCH Verlag GmbH & Co, Weinheim Germany

Coward AJ, Slim AC, Brugger J, Wilson S, Williams T, Pillans B, Maksimenko A (2023) Mineralogy and geochemistry of pattern formation in zebra rock from the East Kimberley, Australia.

Chem Geol 622:121336. https://doi.org/10.1016/j.chemgeo.2023.121336
Cross W, Iddings JP, Pirsson LV, Washington HS (1902/1903). A quantitative chemico-mineralogical classification and nomenclature of igneous rocks (CIPW norm origin)
De Faria DLA, Venâncio Silva S, De Oliveira MT (1997) Raman microspectroscopy of some iron oxides and oxyhydroxides. JRS 28(11):873–878. https://doi.org/10.1002/(SICI)1097-4555(199711)28:11%3C873::AID-JRS177%3E3.0.CO;2-B
Evans BW, Kuehner SM, Joswiak DJ (2021) Pseudomorphic 9-line silician ferrihydrite and Fe-rich serpentine-group minerals in feti oxide-rich ferroan peridotite, Laramie anorthosite complex, Wyoming, USA. Am Mineral 106(6):953–963. https://doi.org/10.2138/am-2021-7768
Ghelardoni R, Pieri M, Pirini C (1965) Osservazioni stratigrafiche nell'area dei Fogli 84 (Pontremoli) e 85 (Castelnuovo ne' Monti). Boll Soc Geol Ital 84(6):297–416
Guimarães WG Jr., Ferreira de Lima G, Anderson Duarte H (2023) Exploring the effect of isomorphically Al-substituted on the thermodynamical and structural properties of hematite and goethite – A DFT investigation. Hydrometallurgy 221(319). https://doi.org/10.1016/j.hydromet.2023.106125
Kawahara H, Yoshida H, Yamamoto K, Katsuta N, Nishimoto S, Umemura A, Kuma R (2022) Hydrothermal formation of Fe-oxide bands in zebra rocks from northern Western Australia. Chem Geol 590:120699. https://doi.org/10.1016/j.chemgeo.2021.120699
Lacchia A, Schuitema G, McAuliffe F (2020) The human side of geoscientists: comparing geoscientists' and non-geoscientists' cognitive and affective responses to geology. GC 3:291–302. https://doi.org/10.5194/gc-3-291-2020
Lan S, Qin Z, Wang X, Yan Y, Tang Y, Feng X, Zhang Q (2021) Kinetics of Mn (II) adsorption and catalytic oxidation on the surface of ferrihydrite. Sci Total Environ 791:148225. https://doi.org/10.1016/j.scitotenv.2021.148225
Liu H, Chen T, Zou X, Qing C, Ray, Frost LR (2013) Effect of al content on the structure of al-substituted goethite: a micro-Raman spectroscopic study. JRS 44(11):1609–1614. https://doi.org/10.1002/jrs.4376
Manceau A, Gates WP (2013) Incorporation of Al in iron oxyhydroxides: implications for the structure of ferrihydrite. Clay Min 48(3):481–489. https://doi.org/10.1180/claymin.2013.048.3.05
Mari R (2018) Pietre Di Giottolandia. Tra spiagge, Greti e Colli Di Maremma Dove La natura imita l'arte. Giunti, Florence Italy
Martini P, Sagri M (1994) The late Miocene-Pleistocene extensional basins of the Northern Apennines: facies distribution and basin fill architecture. Mem Soc Geol Ital 48:375–380
Mazzetti L, Thistlethwaite PJ (2002) Raman spectra and thermal transformations of ferrihydrite and schwertmannite. JRS 33(2):104–111. https://doi.org/10.1002/jrs.830
Mougenot D, Mari R (2021) Toscane - Quand la nature imite l'art: les Giottoli. In: Géochronique, 158. Societe Geologique De France Paris France, pp. 12–15
Ortoleva PJ (1984) The self-organization of Liesegang bands and other precipitate patterns. Chemical instabilities. NATO ASI Series, 120. Springer, Dordrecht Netherlands, pp 289–297. https://doi.org/10.1007/978-94-009-7254-4
Ortoleva PJ (1993) Self-organization and nonlinear dynamics in sedimentary basins. In: Philosophical Transactions of the Royal Society of London. Series A. Physical and Engineering Sciences, 344(1670). Royal Society London England, pp. 171–179
Peccerillo A (2017) Cenozoic Volcanism in the Tyrrhenian Sea Region. Springer International, Berlin, Germany
Sadek S, Sultan R (2010) Liesegang patterns in nature: A diverse scenery across the sciences. Precipitation patterns in reaction-diffusion systems, 661. Research Signpost, Kerala India, pp 1–43
Santo AP, Calandra S, Cappuccini L (2025) Unveiling hidden details of an Etruscan statue: the power of combined pXRF spot and map approach. J Cult Heritage 73:536–542. https://doi.org/10.1016/j.culher.2025.04.031
Schwertmann U (1993) Relations between iron oxides, soil color, and soil formation. Soil color, special publications. Soil Science Society America, Madison, pp 51–69
Schwertmann UTRM, Taylor RM (1989) Iron oxides. In: Minerals in soil environments, Second Edition. Soil Science Society America, Madison, pp. 379–438
Serra M, Borghi A, Gallo LM, Hovoric R, Vaggelli G (2010) Petrographic features, genesis and provenance of Pietra Paesina collections of the Regional Museum of Natural Sciences of Turin, Italy. Period Mineral, Special Issue. https://doi.org/10.2451/2010PM0024
Thomas Arrigo LK, Bouchet S, Kaegi R, Kretzschmar R (2020) Organic matter influences transformation products of ferrihydrite exposed to sulfide. Environ Sci Nano 7(11):3405–3418. https://doi.org/10.1039/d0en00398k
Vai GB, Martini IP (eds) (2001) Anatomy of an orogen: the apennines and adjacent mediterranean basins. Kluwer Academic, Dordrecht, p 632
Vodyanitskii YN, Shoba SA (2016) Ferrihydrite in soils. In: Eurasian Soil Science, 49. Pleiades Publishing, Ltd. Delaware, USA, pp.796–806
Voicu G, Bardoux M, Voicu D (1997) Mineralogical norm calculations applied to tropical weathering profiles. Mineral Mag 61:185–196
Wang A, Freeman JJ, Jolliff BL (2015) Understanding the Raman spectral features of phyllosilicates. JRS 46(10):829–884. https://doi.org/10.1002/jrs.4680
Yoshida H, Katsuta N, Sirono SI, Nishimoto S, Kawahara H, Metcalfe R (2020) Concentric Fe-oxyhydroxide bands in dacite cobbles: rates of buffering chemical reactions. Chem Geol 552:119786. https://doi.org/10.1016/j.chemgeo.2020.119786
Zhao Y, Moore OW, Xiao KQ, Curti L, Fariña AO, Banwart SA, Peacock CL (2022) The role and fate of organic carbon during aging of ferrihydrite. GCA 335:339–355. https://doi.org/10.1016/j.gca.2022.07.003